Target Motion Analysis Using Combined Bearings and Underwater Sound Pressure Levels

Enzo Iglésis, Luc de Montella

Target Motion Analysis Using Combined Bearings and Underwater Sound Pressure Levels

Enzo Iglésis[1] and Luc de Montella*[1,2]

[1] *Inria centre at the University of Bordeaux, Talence, 33405, France*
[2] *Naval Group, Bouguenais, 44340, France.*

November 14, 2024

Abstract

This paper addresses the problem of target motion analysis using underwater sound pressure levels acquired by sonar operating in passive mode. Traditionally, this task is performed using bearing information, and various filtering algorithms, particularly particle filter methods, have shown strong performance in this domain. To improve upon existing approaches, this paper proposes combining bearing information with received noise levels. This approach offers the advantage of avoiding additional sensors compared to bearings-only tracking, as sound pressure levels can be measured with hydrophones, and underwater transmission losses estimated through computational simulations based on commonly available environmental data. The effectiveness of this method, compared to bearings-only tracking, is illustrated using simulated data, showing improved performance even in the absence of observer maneuvers for this challenging nonlinear, multimodal tracking problem.

1 Introduction

Target motion analysis (TMA) is a technique used to estimate the position of a target based on data from passive sensors, such as passive sonar. Passive sonar provides directional information and sometimes frequency data (Maranda, 2008). TMA involves using the direction of incoming sound over time and comparing the target's movement with that of the observer's ownship (Arulampalam *et al.*, 2004; Farina, 1999). In some cases, bearing measurements are supplemented with frequency information to enhance tracking accuracy through Doppler-shifted radiated frequencies (Passerieux *et al.*, 1989; Laneuville, 2007). Nevertheless, TMA remains challenging due to the inherent nonlinearities of the problem and the uncertainties associated with acoustic signal propagation in underwater environments.

Various filtering techniques have been developed to address the complexities of TMA, with particle filters (PFs) emerging as one of the most effective approaches (Arulampalam *et al.*, 2004; Ristic *et al.*, 2019). PFs are well-suited to this problem due to their ability to cope with nonlinear estimation problems. Despite their effectiveness, traditional bearings-only tracking (BOT) methods have limitations, particularly in scenarios where observer maneuvers are restricted due to the noise they generate — which compromises stealthiness (Ovalle and García-Pelaez, 2015) — and negatively affect the processing gain of the passive sonar. In such conditions, bearing measurements alone often lack the necessary information to resolve the target's motion accurately (Nardone and Aidala, 1981).

To overcome these limitations, this paper introduces a novel approach that combines bearing information with received sound pressure level (SPL) measurements. Since sonar systems are essentially transducer arrays, they also measure received SPL (Urick, 1983, chap. 3.4). By incorporating SPL into the tracking process, it is possible to enhance TMA accuracy without the need for additional sensors. This is achieved by estimating underwater transmission losses (TLs) using computational simulations based on environmental data, allowing for the fusion of SPLs data with bearings measurements. The environmental data include the sound speed profile, the bathymetric profile, and the target's frequency. The proposed method improves target tracking performance, particularly in challenging conditions where BOT alone is insufficient.

Since, underwater, sound does not propagate in a straight line due to varying sound speeds with depth — known as the sound speed profile — the resulting TL is often multimodal. This multimodality, combined with the nonlinear nature of the problem, leads to measurements that are both highly nonlinear and ambiguous. These challenges make PFs an

*Luc de Montella would like to thank Naval Group for their financial support through the CIFRE PhD program.

ideal choice for addressing such issues. This problem is analogous to terrain-aided navigation, where specialized PFs have been developed to handle similar complexities (Palmier *et al.*, 2019; Merlinge *et al.*, 2019), many of which could potentially be used to further improve the results presented in this paper.

However, this study does not aim to determine the best filter for this type of problem — an area that has been extensively explored — but rather to demonstrate that incorporating previously unused information can improve solution accuracy. To this end, the filter used is the regularized particle filter (RPF) (Musso *et al.*, 2001), which has been applied to both BOT and TMA with bearing and SPL measurements, providing a fair basis for comparison. The effectiveness of this approach is demonstrated through simulations, showing improved tracking performance compared to traditional BOT methods. Notably, the proposed method performs well even in the absence of observer maneuvers, underscoring its potential for real-world applications.

The remainder of this paper is organized as follows. Section 2 formally defines the TMA problem focusing on BOT. In Section 3, the acoustical emission model of the target and the computation of its TL are detailed to provide a measurement function. Section 4 introduces the RPF that is used for both the BOT and TMA with combined bearing and SPL. The simulation setup and results are presented in Section 5, where the effectiveness of our approach is compared against traditional BOT methods. Finally, Section 6 concludes the paper by summarizing key findings and suggesting directions for future research.

2 Bearing-Only Tracking

Throughout this paper, we assume that the depths of both the observer and the target are known and constant, though not necessarily equal. Therefore, we focus on the two-dimensional version of the BOT problem, as presented in Arulampalam *et al.* (2004, chap. 6)

Consider a Cartesian coordinate system where the positions of the observer and the target at time k are denoted respectively by $\begin{bmatrix} x_k^t & y_k^t \end{bmatrix}^\top$ and $\begin{bmatrix} x_k^o & y_k^o \end{bmatrix}^\top$. We denote the velocity components of the observer and the target at time k respectively by $\begin{bmatrix} \dot{x}_k^t & \dot{y}_k^t \end{bmatrix}^\top$ and $\begin{bmatrix} \dot{x}_k^o & \dot{y}_k^o \end{bmatrix}^\top$. To simplify notation, we define the state vector $\mathbf{x}_k^t$ as

$$\mathbf{x}_k^t = \begin{bmatrix} x_k^t & y_k^t & \dot{x}_k^t & \dot{y}_k^t \end{bmatrix}^\top \tag{1}$$

and the state vector $\mathbf{x}_k^o$ as

$$\mathbf{x}_k^o = \begin{bmatrix} x_k^o & y_k^o & \dot{x}_k^o & \dot{y}_k^o \end{bmatrix}^\top. \tag{2}$$

We let $\mathbf{x}_k$ be the vector representing the position of the target relative to the observer at time k, i. e.,

$$\mathbf{x}_k = \mathbf{x}_k^t - \mathbf{x}_k^o := \begin{bmatrix} x_k & y_k & \dot{x}_k & \dot{y}_k \end{bmatrix}^\top. \tag{3}$$

The target is assumed to have a uniform linear motion. Denoting ΔT as the sampling interval, and $\mathbf{F}$ as the state transition matrix, the state equation can then be written as

$$\mathbf{x}_{k+1} = \mathbf{F}\left(\mathbf{x}_k + \mathbf{x}_k^o\right) - \mathbf{x}_{k+1}^o + \mathbf{\Gamma}\boldsymbol{\nu}_k, \tag{4}$$

where $\mathbf{F}$ is transition matrix given by

$$\mathbf{F} = \begin{bmatrix} 1 & 0 & \Delta T & 0 \\ 0 & 1 & 0 & \Delta T \\ 0 & 0 & 1 & 0 \\ 0 & 0 & 0 & 1 \end{bmatrix}, \tag{5}$$

$\mathbf{\Gamma}$ is the process noise distribution matrix given by

$$\mathbf{\Gamma} = \begin{bmatrix} \frac{\Delta T^2}{2} & 0 \\ 0 & \frac{\Delta T^2}{2} \\ \Delta T & 0 \\ 0 & \Delta T \end{bmatrix}, \tag{6}$$

and $\boldsymbol{\nu}_k \sim \mathcal{N}(0, \mathbf{Q})$ is a white noise with a covariance matrix $\mathbf{Q} = \sigma_a \mathcal{I}_2$ with σ_a the standard deviation of the acceleration process noise and $\mathcal{I}_2$ being the 2×2 identity matrix.

At each time step, the observer obtains a new measurement of the angle between the relative vector $\begin{bmatrix} x_k & y_k \end{bmatrix}^\top$ and the y-axis. This measurement vector, denoted by $\mathbf{z}_k$, is given in the case of BOT by

$$\mathbf{z}_k = \begin{bmatrix} \theta_k \end{bmatrix}, \tag{7}$$

where θ_k denoted the bearing measurement at time step k. It is given by:

$$\theta_k = h_\theta\left(\mathbf{x}_k\right) + \omega_k, \tag{8}$$

where ω_k is a zero-mean independent Gaussian noise with standard deviation σ_θ. The function $h_\theta(\cdot)$ represents the true bearing and is defined as:

$$h_\theta\left(\mathbf{x}_k\right) = \arctan\left(\frac{x_k}{y_k}\right). \tag{9}$$

The BOT problem consists in the estimation of the vectors $\mathbf{x}_k$ given the measurements $\mathbf{Z}_k = \{\mathbf{z}_1, \ldots, \mathbf{z}_k\}$ up to time step k.

3 Source Level and Transmission Loss

As the name suggests, in BOT, the observer relies solely on angular measurements to estimate the target's position, which presents a significant challenge due to the absence of direct range information. Despite this, traditional BOT disregards the received SPL, a potentially critical omission. While the exact distance between the observer and the target remains unknown, knowing the target's source level (SL) and the signal's TL can significantly narrow down the target's potential positions. Indeed, the passive sonar

equation in terms of intensity is given by (Maranda, 2008, chap. 3):

$$\mathrm{SE} = \mathrm{SL} - \mathrm{NL} + \mathrm{AG} - \mathrm{TL} - \mathrm{DT}, \tag{10}$$

where SE, NL, AG, and DT respectively denote the signal excess at the input to the detector, the noise level at the receiver, the array gain of the sensor system relative to an omnidirectional hydrophone, and the detection threshold. In this paper, the sonar is assumed to be ideal, with no array gain (the signal is received with the same intensity regardless of directionality) and no detection threshold (the signal is always received and measured). Therefore, the signal excess then corresponds to the received SPL, which is given by:

$$\mathrm{SPL} = \mathrm{SL} + \mathrm{NL} - \mathrm{TL}\,. \tag{11}$$

To take full advantage of this insight, an accurate model representing both SLs and TLs is essential. In this paper, a simplified NL model is used and will be described later.

3.1 Target Source Level

Assuming that the target's noise propagates isotropically, we use the model presented in Ross (1987, chap. 8.6) to estimate the source level. This model, based on statistical observations of surface ship radiated levels, suggests a linear relationship between the source level and the logarithm of the ship's speed. Using a reference speed of $\approx 5.14\,\mathrm{m\,s^{-1}}$ (10 kn), the resulting trend curve follows this established relationship:

$$\mathrm{SL}\left(\mathbf{x}_k^t\right) = 170 + 53\log\left(\frac{v_k^t}{5.14\,\mathrm{m\,s^{-1}}}\right), \tag{12}$$

with $v_k^t \propto \sqrt{{x_k^t}^2 + {y_k^t}^2}$.

Despite its apparent simplicity, this model has proven to be quite effective, and even recent, more sophisticated models retain this general form (see Wittekind, 2014; Jalkanen *et al.*, 2018). The key difference is that these advanced models incorporate additional tuning parameters, allowing for better adaptation to the specific characteristics of the target.

It is also important to note that filtering methods are used here, rather than inverse methods, making minor inaccuracies in the model less critical. In fact, any errors in the estimation can be viewed as uncertainties within the model, which the filtering process can effectively handle Elfring *et al.* (2021).

3.2 Transmission Loss

The TL can be estimated numerically. In this paper, the TL is obtained using *bellhopcxx* from Pisha *et al.* (2023), an open-source code based on *BELLHOP* (Porter and Bucker, 1987), a widely used beam-tracing model. By specifying environmental data, such as bathymetry and sound speed profiles, ray angles, and other parameters, the model computes the TL at specified receiver positions. *BELLHOP* provides three TL modes: coherent, semi-coherent, and incoherent. The incoherent mode is used in this paper, due to the instability of the detailed fluctuations in the coherent field. *BELLHOP* is capable of producing TL within a 3D environment that accounts for variations in the sound speed profile.

However, for sake of brevity in Section 5 and Appendix, where detailed values are provided, and for computational efficiency, the acoustic environment in this paper is simplified to a flat bottom 2D model. This 2D environment is then interpreted as a flat bottom 3D environment by assuming that sound propagates uniformly in all directions. Therefore, only the range and depth of the receiver are required to compute the TL. The TL function is then denoted

$$\mathrm{TL}\left(\mathbf{x}_k^t, \mathbf{x}_k^o\right). \tag{13}$$

Since *bellhopcxx* produce a TL array at finite position in both range and depth, in this paper, for sake of simplicity and computational efficiency a linear interpolation is performed to estimate values between each point.

3.3 Measurement Equation

At each time step, the observer receives a second observation, denoted l_k, in addition to the bearing angle θ_k. The measurement vector $\mathbf{z}_k$ is then given in the case of combined bearings and SPLs by:

$$\mathbf{z}_k = \begin{bmatrix}\theta_k & l_k\end{bmatrix}^\top. \tag{14}$$

The l_k observation represents the SPL received by the observer, which provides valuable information about the target's emission. The measurement equation of the received SPL is given by:

$$l_k = h_l\left(\mathbf{x}_k^t, \mathbf{x}_k^o\right) + \upsilon_k, \tag{15}$$

where υ_k represents the ambient noise level — previously denoted NL in (10) and (11) —, which is modeled in this paper as Gaussian noise with a mean of zero and a standard deviation σ_l (for more details on ambient ocean noise, see for example Curtis *et al.* (1999) or Urick (1983, chap. 7)). Note that a more realistic noise could be handled here since the PFs are not limited to Gaussian noise unlike Kalman filter (KF)'s approaches, and even considering unknown measurement noise with application-specific PFs as performed in Palmier *et al.* (2019). The function $h_l(\cdot)$ represents the true SPL received. Using (11) it is defined as:

$$h_l\left(\mathbf{x}_k^t, \mathbf{x}_k^o\right) = \mathrm{SL}\left(\mathbf{x}_k^t\right) - \mathrm{TL}\left(\mathbf{x}_k^t, \mathbf{x}_k^o\right). \tag{16}$$

This additional observation l_k complements the bearing angle by providing indirect information about

the distance between the target and the observer, helping to reduce the uncertainty in the target's estimated position.

4 Regularized Particle Filter

Due to its nonlinear nature, the BOT problem has no known exact filter solution. To address this challenge, several modifications of the KF have been proposed. Among these, the extended Kalman filter (EKF) (Anderson and Moore, 2012) and the unscented Kalman filter (UKF) (Julier *et al.*, 2000) are commonly used. Both filters attempt to linearize the nonlinearities inherent in the BOT problem, but they have limitations in terms of accuracy and robustness.

The most effective filters for this problem, however, tend to be variations of the PF(Sindhu *et al.*, 2019; Arulampalam *et al.*, 2004). Their ability to handle nonlinearities and non-Gaussian noise makes them particularly well-suited for the BOT problem. PFs are a class of sequential Monte Carlo methods that use a large number of discrete points, known as particles, to represent the posterior density $p(\mathbf{x}_k \mid \mathbf{z}_k)$. The total number of particles used is denoted N in this paper.

The PF estimates the posterior density using two primary steps: the prediction step (a. k. a. mutation) and the update step (a. k. a. selection). The behavior of these steps, along with potential additional steps, depends on the version of the PF being used. There are numerous variations of PFs, and some produce better results than others, depending on the targeted application. In this paper, the PF chosen is the RPF (Musso *et al.*, 2001), which, in addition to the two primary steps mentioned above, includes a regularization-resampling step. This filter was selected because it is widespread and efficient without being application-specific. It is important to note that some algorithms could be better suited to the problem at hand. For example, many algorithms developed for terrain-aided navigation have demonstrated improved performance in comparable scenarios. These algorithms, designed to match environmental data with real-time sensor inputs, could also prove highly effective for our application (see Ma *et al.*, 2023; Palmier *et al.*, 2019; Merlinge *et al.*, 2019). However, evaluating and determining the optimal algorithm for this specific problem is beyond the scope of this paper. For this reason, the RPF has been chosen for our simulations, providing a balanced approach between complexity and effectiveness.

4.1 Prediction Step

This step aims to propagate the particles using the following probability transition density:

$$\mathbf{x}_{k|k-1}^{(i)} \sim p\left(\mathbf{x}_{k|k-1} \mid \mathbf{x}_{k-1}^{(i)}\right), \tag{17}$$

where the superscript (i) denotes the i^{th} particle. This probability transition density is determined by the dynamics of the system. Each particle then independently evolves according to the state equation (4).

4.2 Update Step

In a PF, each particle is assigned a weight, denoted here by w, which is proportional to the likelihood of the new observation. This effectively adjusts the particles to better fit the observed data. The weight of the i^{th} particle is given by

$$\tilde{w}_k^{(i)} \propto w_{k-1}^{(i)} p\left(\mathbf{z}_k \mid \mathbf{x}_{k|k-1}^{(i)}\right). \tag{18}$$

To ensure that $\sum_{i=1}^{N} w_k^{(i)} = 1$, a normalization is performed, which gives

$$w_k^{(i)} = \frac{\tilde{w}_k^{(i)}}{\sum_{i=1}^{N} \tilde{w}_k^{(i)}}. \tag{19}$$

4.3 Regularization-Resampling Step

If the variance of the weights becomes too large, it indicates that a few particles dominate the distribution, which is known as the degeneracy problem. To counteract this, a resampling process is performed to remove particles with small weights and duplicate those with large weights. To evaluate the variance of the weights, a criterion is compared to a user-defined threshold, denoted N_{thr}, to determine if a resampling step is needed. The criterion used in this paper is the efficiency (Kong *et al.*, 1994), denoted N_{eff}, and computed as follows:

$$N_{eff} = \frac{1}{\sum_{i=1}^{N} {w_k^{(i)}}^2}. \tag{20}$$

If $N_{eff} < N_{thr} N$, the regularization-resampling step is performed. The first stage of this step is the resampling step, which aims to draw a new set of particles from the existing set, with probabilities proportional to their weights. This resampling stage improves the accuracy of the state estimation by concentrating computational resources on the most likely particles while discarding the less likely ones. However, this multinomial draw duplicates particles, which reduces diversity.

The second stage of this step addresses this by performing regularization. Regularization involves adding independent noise to each particle, which helps maintain diversity within the particle set. By preventing the particles from collapsing into a small number of concentrated regions, this step improves the overall approximation of the posterior distribution and

enhances the filter's performance, especially in high-dimensional or challenging environments. The independent noise applied to the particles is performed according to a regularization kernel $\mathcal{K}(\cdot)$. The regularization equation is:

$$\mathbf{x}_k^{(i)} = \acute{\mathbf{x}}_k^{(i)} + h\mathbf{D}_k\boldsymbol{\varepsilon}^{(i)}, \tag{21}$$

where the covariance matrix $\mathbf{P}_k = \mathbf{D}_k\mathbf{D}_k^\top$, $\boldsymbol{\varepsilon}^{(i)} \sim \mathcal{K}(\cdot)$ and $\acute{\mathbf{x}}$ is the output vector of the multinomial draw. The kernel density is a symmetric probability density function such that:

$$\int \mathbf{x}\mathcal{K}(\mathbf{x})\, d\mathbf{x} = 0, \quad \int \|\mathbf{x}\|^2\mathcal{K}(\mathbf{x})\, \mathrm{d}\mathbf{x} < \infty. \tag{22}$$

The kernel $\mathcal{K}(\cdot)$ and the bandwidth h (a scalar parameter) are selected to minimize the mean integrated square error (MISE) between the true posterior density and the corresponding empirical representation, which is given by:

$$\mathrm{MISE}(\hat{p}) = \mathbb{E}\left(\int \left(p(\mathbf{x}_k|\mathbf{Z}_k) - \hat{p}(\mathbf{x}_k|\mathbf{Z}_k)\right)^2 \mathrm{d}\mathbf{x}_k\right), \tag{23}$$

where $\hat{p}(\mathbf{x}_k|\mathbf{Z}_k)$ denotes the approximation to $p(\mathbf{x}_k|\mathbf{Z}_k)$ and is given by:

$$\hat{p}(\mathbf{x}_k|\mathbf{Z}_k) = \sum_{i=1}^{N} w_k^{(i)} \mathcal{K}_h\left(\mathbf{x}_k - \mathbf{x}_k^{(i)}\right). \tag{24}$$

The regularization kernel $\mathcal{K}_h(\cdot)$ is given by:

$$\mathcal{K}_h(\mathbf{x}) = \frac{1}{h^{n_x}}\mathcal{K}\left(\frac{\mathbf{x}}{h}\right), \tag{25}$$

where $h \in \mathbb{R}^{+*}$ is the kernel bandwidth for the rescaled kernel density $\mathcal{K}(\cdot)$ and n_x the dimension of the state vector $\mathbf{x}$.

The Epanechnikov kernel is chosen as an optimal kernel (Silverman, 2018) and is given by:

$$\mathcal{K}(\mathbf{x}) = \begin{cases} \frac{n_x+2}{2c_{n_x}}\left(1 - \|\mathbf{x}\|^2\right) & \text{if} \quad \|\mathbf{x}\| < 1 \\ 0 & \text{else} \end{cases}, \tag{26}$$

where c_{n_x} is the unit hypersphere volume in $\mathbb{R}^{n_x}$.

The MISE optimal bandwidth is then given by (Silverman, 2018):

$$h = A(\mathcal{K})\, N^{-\frac{1}{n_x+4}}, \tag{27}$$

with

$$A(\mathcal{K}) = \left(8c_{n_x}^{-1}(n_x+4)\left(2\sqrt{\pi}\right)^{n_x}\right)^{\frac{1}{n_x+4}}. \tag{28}$$

4.4 Estimation Output

The global estimate of the state vector $\mathbf{x}_k$ denoted $\hat{\mathbf{x}}_k$ and its associated estimated covariance matrix denoted $\hat{\mathbf{P}}_k$ are respectively given by:

$$\hat{\mathbf{x}}_k = \sum_{i=1}^{N} w_k^{(i)}\mathbf{x}_k^{(i)} \tag{29}$$

and

$$\hat{\mathbf{P}}_k = \sum_{i=1}^{N} w_k^{(i)}\left(\mathbf{x}_k^{(i)} - \hat{\mathbf{x}}_k\right)\left(\mathbf{x}_k^{(i)} - \hat{\mathbf{x}}_k\right)^\top. \tag{30}$$

In this paper, the global estimate is computed after the regularization-resampling step, whether or not the step is performed.

4.5 Regularized Particle Filter for Target Motion Analysis

Another significant advantage of this method is its ease of extension from the traditional BOT problem to TMA with combined bearing and SPL measurements. The adaptation is straightforward, requiring only a modification of the likelihood function to incorporate the noise level data. Given the positions of both the target and the observer, the angle measurement and the noise level measurement can be considered independent. As a result, the likelihood can be computed by combining the two independent observations as follows:

$$p(\mathbf{z}_k \,|\, \mathbf{x}_k,\, \mathbf{x}_k^o) = p(\theta_k \,|\, \mathbf{x}_k,\, \mathbf{x}_k^o)p(l_k \,|\, \mathbf{x}_k,\, \mathbf{x}_k^o), \tag{31}$$

with $p(\theta_k \,|\, \mathbf{x}_k,\, \mathbf{x}_k^o)$ and $p(l_k \,|\, \mathbf{x}_k,\, \mathbf{x}_k^o)$ respectively proportional to:

$$p(\theta_k \,|\, \mathbf{x}_k,\, \mathbf{x}_k^o) \propto \exp\left(-\frac{\left(\theta_k - h_\theta(\mathbf{x}_k)\right)^2}{2\sigma_\theta^2}\right) \tag{32}$$

and

$$p(l_k|\, \mathbf{x}_k,\, \mathbf{x}_k^o) \propto \exp\left(-\frac{\left(l_k - h_l(\mathbf{x}_k + \mathbf{x}_k^o,\, \mathbf{x}_k^o)\right)^2}{2\sigma_l^2}\right). \tag{33}$$

It is assumed that the initial state of the target is modeled by a Gaussian distribution.

5 Numerical Results

The scenarios used in the simulations are directly based on those described in Ristic *et al.* (2003, chap. 6). However, in Subsections 5.2 and 5.3, the observer trajectory is modified and the time horizon is extended to provide a more complete visualization of the results.

In all scenarios, the observer starts at a depth of 300 m at the position [0 0] in a Cartesian coordinate system where the coordinates are measured in meters. The target is initially positioned at [5000 800] with a depth of 5 m. It maintains a constant speed of $\approx$2.57 m s^{-1} (5 kn) and a steady course of $-140°$. The process noise σ_a is set to 1.5×10^{-3} m s^{-2}.

The particles are initialized with a prior distribution for the range centered at 10 km with a standard deviation of 2 km. The initial direction is determined

by the first angle measurement, with the angular variance σ_θ set to 1.5°. The initial speed is drawn from a Gaussian distribution centered at $\approx$1.54 m s^{-1} (3 kn), with a standard deviation of $\approx$1.03 m s^{-1} (2 kn). The initial course is set to $z_0 + \pi$ with a standard deviation of $\pi/\sqrt{12}$. The complete initialization procedure is detailed in Ristic *et al.* (2003, chap. 6.4.1.1).

The filters use $N = 5000$ particles, with a resampling threshold N_{thr} set to $N/3$. A measure is received every 60 s. Although the noise in the signal level is generated with a standard deviation σ_l of 4 dB, the likelihood function within the filter is computed under the assumption that the standard deviation is 10 dB. This introduces more flexibility into the algorithm and results in improved performance.

The bottom of the environment is set at 1000 m, with a target radiating at 50 Hz. The sound speed profile is a Munk profile (Porter, 2011, chap. 4). This profile, along with other parameters used within the *bellhopcxx* input environmental data file, is provided in Appendix. The resulting transmission loss is illustrated in FIG. 1.

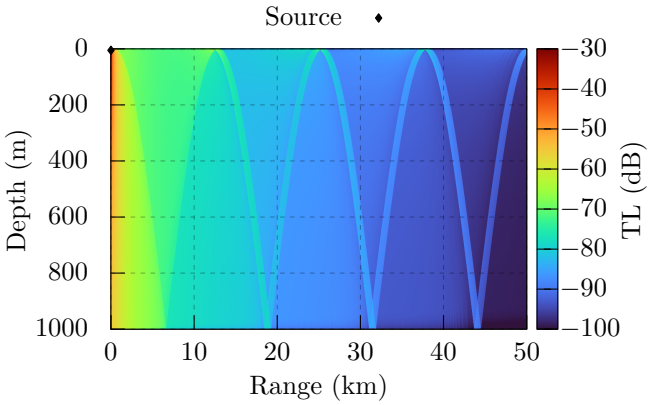

Figure 1: Side view of transmission loss with the environmental data of Appendix using incoherent Gaussian beams.

For each simulation, we present the evolution of the root-mean-square error (RMSE) for the target's position over 1000 runs, comparing both BOT and TMA using combined bearing and SPL measurements. An SPL-only tracking method was also tested, but it failed to track the target. Due to its divergence, the RMSE for this method has been excluded from the figures to improve clarity. Alongside the RMSEs, we include the Cramér-Rao lower bounds (CRLB) for the BOT problem, assuming zero process noise. The detailed derivation of this bound can be found in Ristic *et al.* (2003, chap. 4.3.3). It is important to note that this bound applies specifically to the classical BOT problem, and there is no theoretical restriction preventing the RMSE from falling below this bound when SPLs are considered.

5.1 Maneuvering Observer

In these simulations, the observation period lasts 30 min. The observer travels at a constant speed of $\approx$2.57 m s^{-1} (5 kn). It starts with an initial course of 140° and executes a maneuver between 13 min and 17 min to attain a new course of 20°. The observer maintains this new course for the remainder of the observation period. This scenario is illustrated in FIG. 2.

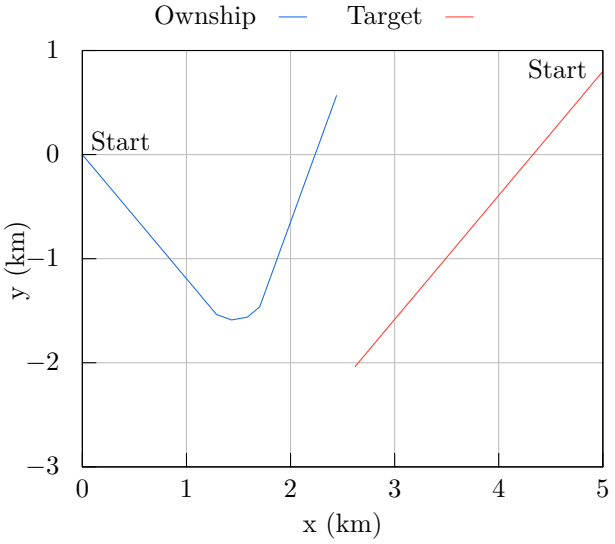

Figure 2: Scenario with maneuvering ownship.

The evolution of the RMSEs throughout this time frame is illustrated in FIG. 3.

Before the maneuver, the RMSEs of both the classical BOT and the TMA with combined bearings and SPLs follow a similar upward trend. During the maneuver, however, both methods show a sharp decrease in RMSE. Note that the TMA with combined bearings and SPLs reaches lower RMSE values both during and after this drop, indicating greater accuracy compared to the classical BOT. At 24 min the minimum RMSE value is reached in this scenario for both classical BOT and TMA with combined bearings and SPLs, with respectively 155 m and 85 m. This represents an improvement of 54.71 % for the TMA with combined bearings and SPLs over the classical BOT.

Although the RMSEs of both methods rise again following the maneuver, the TMA with combined bearings and SPLs consistently maintains lower values through the remainder of the scenario. This suggests that incorporating noise level information not only enhances the value of high-quality bearing data, especially during the maneuver, but also helps stabilize tracking and provides more robust estimates over time, particularly when the observer moves in a straight line and the bearing information becomes less reliable.

The final RMSE values for the classical BOT and

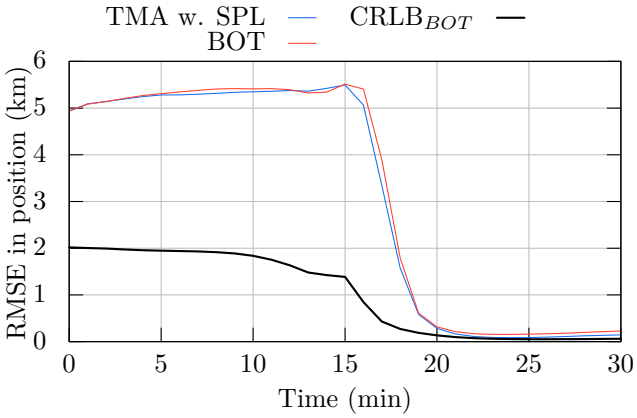

(a) Time Interval: 0 min to 30 min.

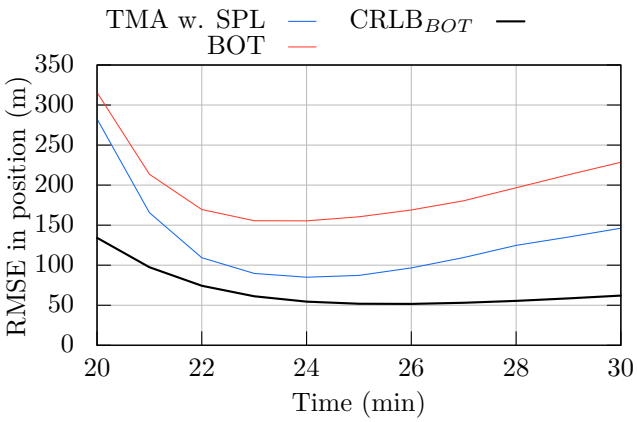

(b) Detailed View: 20 min to 30 min.

Figure 3: Evolution of RMSE for BOT with a maneuvering observer.

the TMA with combined bearings and SPLs are 228.58 m and 146.17 m, respectively. Therefore, in this scenario, neglecting noise level information results in a 156.37 % deterioration in RMSE performance.

5.2 Non-Maneuvering Observer

In these simulations, the observation period lasts 150 min. The observer travels at a constant speed of $\approx$2.57 m s^{-1} (5 kn) on a course of $-140°$, traveling parallel to the target. In this specific configuration, the quality of bearing data is significantly degraded. The near-zero bearing rate further complicates the situation, making it impossible for standard BOT methods to yield accurate or reliable estimates. As a result, the traditional BOT problem becomes unobservable (see Nardone *et al.*, 1984), making it a challenging scenario for the TMA with combined bearing and SPLs. This scenario is illustrated in FIG. 4.

As shown in FIG. 5, traditional BOT methods struggle to handle poor data quality, leading to consistent divergence and increasingly inaccurate estimates over time. This degradation over time is also reflected in the steady rise of the CRLB of the BOT, highlighting that, in this scenario, bearing information alone is insufficient for precise target position estimation.

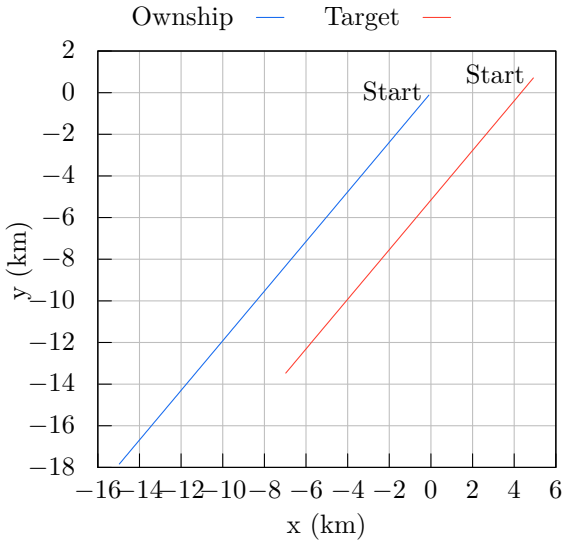

Figure 4: Scenario with non-maneuvering ownship.

However, incorporating SPLs data helps mitigate these issues. By combining bearing measurements with SPLs information, the tracking system is not only able to avoid the divergence of the error, but it also maintains a more stable and bounded error.

Even more striking, the method's RMSE decreases consistently enough that, after around 140 min, the RMSE falls below the CRLB of the BOT. This scenario highlights the importance of taking SPLs data into account when bearing information is poor.

Despite being initializes in the same way, neglecting SPLs data results in a degradation of 477.43 % of the estimate after 150 min.

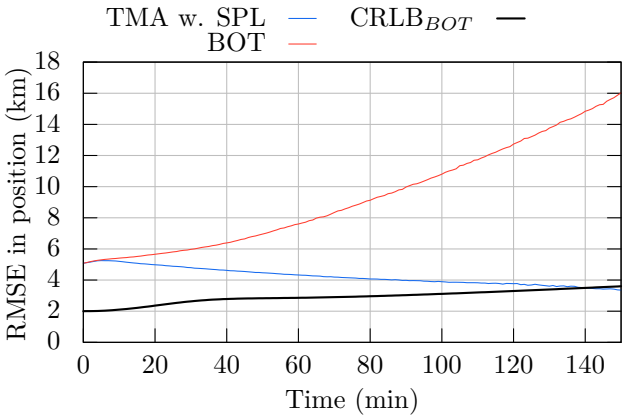

Figure 5: Evolution of RMSE for BOT with a Non-Maneuvering Observer

5.3 Static Observer

In these simulations, the observation period extends over 150 min, with the observer remaining stationary at its initial position throughout the entire duration. Similar to the non-maneuvering observer scenario, the bearing information is of poor quality and the classical BOT problem is unobservable. This scenario is illustrated in FIG. 6.

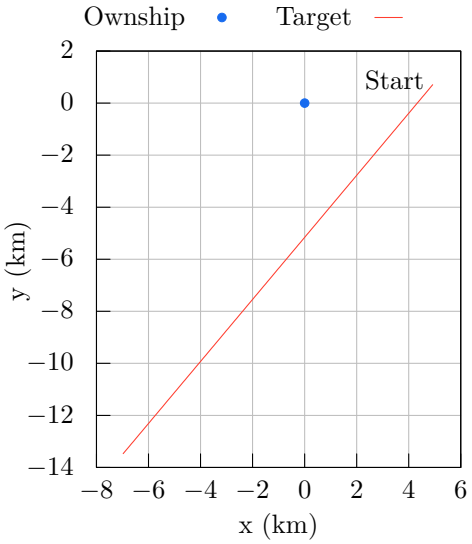

Figure 6: Scenario with static ownship.

As illustrated by the evolution of the RMSEs in FIG. 7, both the BOT and the TMA with combined bearings and SPLs exhibit improvement in estimation quality during the initial 36 min at which point the BOT reached its lowest RMSE value of 2857 m while the TMA with combined bearings and SPLs is already at 344 m. For the BOT method, the estimation error increases steadily after this period, eventually leading to a complete loss of target tracking. In contrast, when SPLs data is incorporated, the estimation quality remains stable until approximately 100 min and reach it lowest RMSE value at 63 min with 203 m while the BOT is at 4338 m. Although a gradual increase in error does occur after this point, it is significantly less severe than the rapid deterioration observed in the BOT approach.

Beyond the overall improved performance when considering SPLs, the most notable observation is that the RMSE in this case actually falls well below the CRLB of the BOT. In fact, while neglecting SPLs leads to a 891.69 % degradation in estimation accuracy by the final time step, the CRLB of the BOT itself is 313.88 % higher than the RMSE obtained when using both bearings and SPLs. These RMSEs value of this scenario are summarized in TABLE 1.

This significant improvement highlights the potential of the method and is a highly encouraging result for future applications.

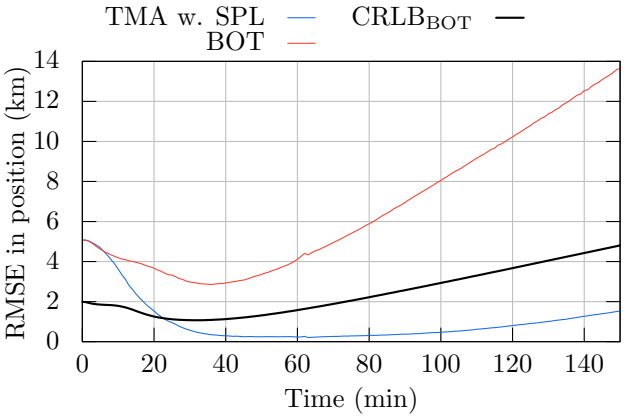

Figure 7: Evolution of RMSE for BOT with a Static Observer

Table 1: RMSEs values for the static observer at time of the minimum RMSEs value reached (underlined value) for each algorithm and final time.

Algorithm	RMSE		
	36 min	63 min	150 min
BOT	<u>2857 m</u>	4338 m	13 657 m
TMA w. SPL	344 m	<u>203 m</u>	1532 m

6 Conclusion

This paper presented a comparative study of TMA using combined bearing and SPL measurements versus traditional BOT. Three different scenarios were evaluated: maneuvering ownship, non-maneuvering ownship, and static ownship. The results consistently demonstrate the superior performance of combining bearings with SPLs compared to conventional BOT, highlighting its potential for real-world applications. SPL measurements proved especially valuable in scenarios with poor bearing information quality, as they not only prevented estimation divergence but also reduced estimation error over time. In fact, the observed RMSE for the method incorporating SPL even falls below the CRLB for BOT in such cases.

It is important to note that these results assume the sound speed profile is known, which is often the case when sonar systems are used. For future work, simulations could be extended to a more realistic 3D environment with varying sound speed profiles, offering a more comprehensive analysis.

Another limitation of this study is the assumption that the target's depth is known. While this is not a major issue when dealing with surface ships, it could pose challenges in other scenarios. Additionally, this study focused on targets in rectilinear motion at constant speed, avoiding the introduction of filter-dependent parameters that could complicate the

comparison, but the use of this approach on maneuvering targets with specialized filters could be promising and provide interesting results.

A significant limitation is the assumption of an isotropically radiating source, neglecting the directivity index, which could impact the performance of the method in more complex acoustic environments. Future research could address these issues to further refine the approach.

A BELLHOP Environmental Data

The environmental data use as input of *bellhopcxx* are the following:

```
Munk profile                ! TITLE
50.0                        ! FREQ
1                           ! NMEDIA
CVM                         ! SSPOPT
51  0.0  1000              ! DEPTH
    0.0  1548.52  0.0 /
  200.0  1530.29  0.0 /
  250.0  1526.69  0.0 /
  400.0  1517.78  0.0 /
  600.0  1509.49  0.0 /
  800.0  1504.30  0.0 /
 1000.0  1501.38  0.0 /
A 0.0                        ! Bottom model
1000.0 1600.0 0.0 1.8 0.8 / ! Halfspace
1                           ! NSD
5 /                         ! SD(1:NSD)
1000                        ! NRD
0.0 999.0 /                 ! RD(1:NRD)
5000                        ! NR
0.0 49.99 /                 ! R(1:NR)
IG                          ! Run type
0                           ! NBEAMS
-90.0 90.0 /                ! ALPHA
0.0 1800.0 50.09            ! STEP, ZBOX, RBO
```

References

Anderson, B., and Moore, J. (**2012**). Dover Books on Electrical Engineering *Optimal Filtering* (Dover Publications).

Arulampalam, S., Ristic, B., Gordon, N., and Mansell, T. (**2004**). "Bearings-only tracking of manoeuvring targets using particle filters," EURASIP Journal on Advances in Signal Processing **2004**, 1–15.

Curtis, K., Howe, B., and Mercer, J. (**1999**). "Low-frequency ambient sound in the North Pacific: Long time series observations," The Journal of the Acoustical Society of America **106**(6), 3189–3200.

Elfring, J., Torta, E., and van de Molengraft, R. (**2021**). "Particle filters: A hands-on tutorial," Sensors **21**(2).

Farina, A. (**1999**). "Target tracking with bearings–only measurements," Signal processing **78**(1), 61–78.

Jalkanen, J.-P., Johansson, L., Liefvendahl, M., Bensow, R., Sigray, P., Östberg, M., Karasalo, I., Andersson, M., Peltonen, H., and Pajala, J. (**2018**). "Modelling of ships as a source of underwater noise," Ocean Science **14**(6), 1373–1383.

Julier, S., Uhlmann, J., and Durrant-Whyte, H. (**2000**). "A new method for the nonlinear transformation of means and covariances in filters and estimators," IEEE Transactions on Automatic Control **45**(3), 477–482.

Kong, A., Liu, J. S., and Wong, W. H. (**1994**). "Sequential imputations and bayesian missing data problems," Journal of the American statistical association **89**(425), 278–288.

Laneuville, D. (**2007**). "Target motion analysis with passive data fusion," .

Ma, T., Ding, S., Li, Y., and Fan, J. (**2023**). "A review of terrain aided navigation for underwater vehicles," Ocean Engineering **281**, 114779.

Maranda, B. (**2008**). *Passive Sonar*, 1757–1781 (Springer New York, New York, NY).

Merlinge, N., Dahia, K., Piet-Lahanier, H., Brusey, J., and Horri, N. (**2019**). "A box regularized particle filter for state estimation with severely ambiguous and non-linear measurements," Automatica **104**, 102–110.

Musso, C., Oudjane, N., and Le Gland, F. (**2001**). *Improving Regularised Particle Filters*, 247–271 (Springer New York, New York, NY).

Nardone, S., and Aidala, V. (**1981**). "Observability criteria for bearings-only target motion analysis," IEEE Transactions on Aerospace and Electronic Systems **AES-17**(2), 162–166.

Nardone, S., Lindgren, A., and G., K. (**1984**). "Fundamental properties and performance of conventional bearings-only target motion analysis," IEEE Transactions on Automatic Control **29**(9), 775–787.

Ovalle, D., and García-Pelaez, J. (**2015**). "Minimizing underwater noise generated by submarine maneuvering: an optimal control approach," IEEE Journal of Oceanic Engineering **41**(2), 362–372.

Palmier, C., Dahia, K., Merlinge, N., Del Moral, P., Laneuville, D., and Musso, C. (**2019**). "Adaptive approximate bayesian computational particle filters

for underwater terrain aided navigation," in *2019 22th International Conference on Information Fusion (FUSION)*, IEEE, pp. 1–8.

Passerieux, J., Pillon, D., Blanc-Benon, P., and Jauffret, C. (**1989**). "Target motion analysis with bearings and frequencies measurements via instrumental variable estimator (passive sonar)," in *International Conference on Acoustics, Speech, and Signal Processing,*, pp. 2645–2648 vol.4.

Pisha, L., Snider, J., Jackson, K., and Jaffe, J. (**2023**). "Introducing bellhopcxx/bellhopcuda: Modern, parallel bellhop(3d)," The Journal of the Acoustical Society of America **153**(3 supplement), A218–A218.

Porter, M., and Bucker, H. (**1987**). "Gaussian beam tracing for computing ocean acoustic fields," The Journal of the Acoustical Society of America **82**(4), 1349–1359.

Porter, M. B. (**2011**). "The bellhop manual and user's guide: Preliminary draft," Heat, Light, and Sound Research, Inc., La Jolla, CA, USA, Tech. Rep **260**.

Ristic, B., Arulampalam, S., and Gordon, N. (**2003**). *Beyond the Kalman Filter: Particle Filters for Tracking Applications* (Artech House).

Ristic, B., Houssineau, J., and Arulampalam, S. (**2019**). "Robust target motion analysis using the possibility particle filter," IET Radar, Sonar & Navigation **13**(1), 18–22.

Ross, D. (**1987**). *Mechanics of Underwater Noise* (Peninsula Publishing).

Silverman, B. W. (**2018**). *Density estimation for statistics and data analysis* (Routledge).

Sindhu, B., Jayaraman, V., and Christopher, S. (**2019**). "Bearing only target tracking using single and multisensor: A review," Journal of Engineering Science and Technology Review **12**, 50–65.

Urick, R. (**1983**). *Principles of underwater sound — 2. ed.* (Peninsula Publishing).

Wittekind, D. (**2014**). "A simple model for the underwater noise source level of ships," Journal of Ship Production and Design **30**.